HHS Public Access

Author manuscript

Exp Neurol. Author manuscript; available in PMC 2021 January 01.

Published in final edited form as:

Exp Neurol. 2020 January ; 323: 113111. doi:10.1016/j.expneurol.2019.113111.

The role of BTBD9 in the cerebral cortex and the pathogenesis of restless legs syndrome

Shangru Lyu[1], **Hong Xing**[1], **Mark P. DeAndrade**[1], **Pablo D. Perez**[2], **Keer Zhang**[1], **Yuning Liu**[1], **Fumiaki Yokoi**[1], **Marcelo Febo**[2], **Yuqing Li**[1,*]

[1]Norman Fixel Institute for Neurological Diseases, Department of Neurology, College of Medicine, University of Florida Gainesville, Florida, USA

[2]Department of Psychiatry, College of Medicine, University of Florida Gainesville, Florida, USA

Abstract

Restless legs syndrome (RLS) is a nocturnal neurological disorder affecting up to 10%of the population. It is characterized by an urge to move and uncomfortable sensations in the legs which can be relieved by movements. Mutations in *BTBD9* may confer a higher risk of RLS. We developed *Btbd9* knockout mice as an animal model. Functional alterations in the cerebral cortex, especially the sensorimotor cortex, have been found in RLS patients in several imaging studies. However, the role of cerebral cortex in the pathogenesis of RLS remains unclear. To explore this, we used *in vivo* manganese-enhanced MRI and found that the *Btbd9* knockout mice had significantly increased neural activities in the primary somatosensory cortex (S1) and the rostral piriform cortex. Morphometry study revealed a decreased thickness in a part of S1 representing the hindlimb (S1HL) and M1. The electrophysiological recording showed *Btbd9* knockout mice had enhanced short-term plasticity at the corticostriatal terminals to D1 medium spiny neurons (MSNs). Furthermore, we specifically knocked out *Btbd9* in the cerebral cortex of mice (*Btbd9* cKO). The *Btbd9* cKO mice showed a rest-phase specific motor restlessness, decreased thermal sensation, and a thinner S1HL and M1. Both *Btbd9* knockout and *Btbd9* cKO exhibited motor deficits. Our results indicate that systematic BTBD9 deficiency leads to both functional and morphometrical changes of the cerebral cortex, and an alteration in the corticostriatal pathway to D1 MSNs. Loss of BTBD9 only in the cerebral cortex is sufficient to cause similar phenotypes as observed in the *Btbd9* complete knockout mice.

Keywords

Restless legs syndrome; *Btbd9*; cerebral cortex; cortical thickness; corticostriatal pathway

Introduction

Restless leg syndrome (RLS) is a sensorimotor neurological disease that affects up to 10% of the general population. Characteristic sensory symptoms of RLS include an urge to move

[*]***Corresponding author at:*** Department of Neurology, College of Medicine, University of Florida, PO Box 100236, Gainesville, Florida 32610-0236; yuqing.li@neurology.ufl.edu.

Declarations of interest: none

and uncomfortable sensations commonly in the lower limbs, which can be relieved by movements like walking and stretching (Garcia Borreguero et al., 2017). Mostly occurring at night, RLS causes perturbation of the sleep cycle and impacts the patient's overall quality of life (DeAndrade et al., 2012a). Although not being fully understood, the pathophysiology underlying the RLS is thought to be related to dysfunctional iron metabolism and dysregulated dopamine (DA) system (Ferre et al., 2019; Khan et al., 2017).

Structural alterations have been reported in the cerebral cortex of RLS patients in several imaging studies (Bucher et al., 1997; Celle et al., 2010; Chang et al., 2015; Comley et al., 2012; Connor et al., 2011; Etgen et al., 2005; Hornyak et al., 2007; Lee et al., 2018; Margariti et al., 2012; Pan et al., 2014; San Pedro et al., 1998; Scalise et al., 2004; Scalise et al., 2010; Tyvaert et al., 2009; Unrath et al., 2007; Unrath et al., 2008). RLS patients have been found to have significantly decreased regional gray matter volume in the bihemispheric primary somatosensory cortex, which extended into left-sided primary motor areas (Unrath et al., 2007). In addition, RLS patients show altered white matter properties, including fiber density, axonal diameter, and myelination, in brain regions connected to somatosensory and motor/premotor cortical areas (Unrath et al., 2008). Recently, RLS patients were shown to have thinner brain tissue in the primary somatosensory cortex and fewer connections in the somatosensory pathway (Lee et al., 2018). These clinical observations suggest that symptoms of RLS may be associated with cortical sensorimotor dysfunction (Tyvaert et al., 2009). Moreover, the iron-deficient rats show hypersensitive corticostriatal glutamatergic terminals, which indicates a functional alteration in the corticostriatal neurotransmission (Yepes et al., 2017). However, the role of cerebral cortex in the pathogenesis of RLS is still unknown.

Genome-wide association studies (GWAS) have implicated up to 19 risk loci, including *BTBD9*, as genetic risk factors of RLS (Schormair et al., 2017; Winkelmann et al., 2007). Our knowledge about the physiological roles of BTBD9 is limited. It has been known that *BTBD9* codes for a protein belonging to the BTB (POZ) protein family, which modulates protein ubiquitination (Stogios et al., 2005). Alterations in hippocampal synaptic plasticity and neurotransmission have been found in *Btbd9* knockout (KO) mice (DeAndrade et al., 2012b). Although there is no evidence for a decrease in the functioning of *BTBD9* in human RLS, loss of the *BTBD9* homolog in *Drosophila melanogaster* results in increased motor activity, decreased DA levels, and disrupted sleep patterns (Freeman et al., 2012) akin to human RLS. Similarly, *Btbd9* KO mice showed motor restlessness, thermal hypersensitivity, and a disruption in the sleep structure (DeAndrade et al., 2012a). Therefore, *Btbd9* KO can be considered as a valuable disease model to study the pathophysiology of RLS (Allen et al., 2017).

To understand the role of cerebral cortex in the pathophysiology of RLS, we performed *in vivo* manganese-enhanced magnetic resonance imaging (MEMRI) with our *Btbd9* KO mice and mapped their cerebral cortical activity. We also compared the morphology of the somatosensory cortex, primary motor cortex, and corpus callosum between the *Btbd9* KO mice and their wild type (WT) littermates. Paired-pulse facilitation (PPF) at the D1 corticostriatal terminals was then measured. Finally, we conditionally deleted *Btbd9* in the cerebral cortex and conducted behavioral and morphological tests.

Material and methods

Mice

All animal experiments comply with the ARRIVE guidelines were carried out following the National Institutes of Health guide for the care and use of laboratory animals (NIH Publications No. 8023, revised 1978). All animals used were adult males about 3 to 15 months of age, unless otherwise specifically indicated.

The generation of Btbd9 KO mice—The *Btbd9* KO mice used in the imaging study were generated as described previously (DeAndrade et al., 2012a). *Btbd9* KO mice used in the histology and electrophysical recordings were generated from a line of mice imported from the European Mouse Mutant Archive (EMMA) (EMMA ID: 05554). In this line, the 4th exon of the *Btbd9* gene is flanked by *loxP* sites (floxed). We first removed the neomycin selection cassette by crossing with FLP mice (Jackson Laboratory stock no. 003946) to obtain *Btbd9 loxP* breeders, which was then crossed with the *Emx1-cre* mice, with *cre* directly inserted into the downstream of putative *Emx1* promoter (Guo et al., 2000). Double heterozygous male mice were then crossed with homozygous *Btbd9 loxP* female mice. *Emx1* expresses in the testis germ cells (Yue et al., 2014). Therefore, when the sperms contained both *Emx1-cre* and *Btbd9 loxP*, the recombination occurred and led to a deletion of the targeted sites. The offspring generated from this sperm had a *Btbd9* heterozygous KO locus. Heterozygous *Btbd9* KO mice were either interbred directly or bred with the *Drd1-EGFP* mice (MMRRC stock no. 000297-MU) to generate *Drd1-EGFP Btbd9* KO double heterozygous mice, which were then bred with heterozygous *Btbd9* KO mice to produce the experimental heterozygous *Drd1-EGFP* and homozygous *Btbd9* KO mice, and the heterozygous *Drd1-EGFP* control littermates. Mice were housed in standard mouse cages (29 × 18 × 13 cm; up to 5 mice with the same gender) at 72°F under normal 12-hour light, 12-hour dark cycle (12 LD) condition.

The generation of cerebral cortex-specific Btbd9 knockout mice—The cerebral cortex-specific *Btbd9* knockout mice (*Btbd9* cKO) were generated by crossing *Btbd9 loxP* mice with *Emx1-cre* mice. Double heterozygous female mice (*Emx1-cre*+/−*Btbd9 loxP*+/−) were then crossed with homozygous *Btbd9 loxP* male mice (*Btbd9 loxP*−/−). The offsprings whose genotypes were *Emx1-cre*+/−*Btbd9 loxP*−/− were used as experimental animals. *Btbd9 loxP*+/− or *Btbd9 loxP*−/− littermates were used as controls. PCR was used for genotyping the *Emx1-cre* (forward: ATC TCC GGT ATT GAA ACT CCA GCG C; reverse: CAC TCA TGG AAA ATA GCG ATC) and the *loxP* sites (forward: ACA TCA CCC ATT ACT TAG AAC CTC; reverse: CAC AGC TAT TTC CTG TCA TTC TGG ACA).

Manganese-enhanced magnetic resonance imaging (MEMRI)

Manganese Chloride ($MnCl_2$) pretreatment—A total of 6 adult *Btbd9* KO and 8 WT littermates were used in brain imaging. Before the treatment, the animals used in the experiment were handled every day for 2 weeks and acclimatized to the investigator. Manganese (II) chloride tetrahydrate was purchased from Sigma-Aldrich Chemical Co. (St. Louis, MO, USA), dissolved in distilled deionized water and sterilely filtered before

administered intraperitoneally at a dose of 70 mg/kg/ml. After injections, mice were returned to their home cage and imaged in the next 20–24 h.

Magnetic resonance imaging (MRI)—Images were collected by a 4.7 Tesla Magnex Scientific scanner under the control of Agilent Technologies VnmrJ 3.1 console software. A 38-mm quadrature transmit/receive radiofrequency coil tuned to 200MHz was used (Insight NeuroImaging Systems, LLC, Leominster, MA). Mice were anesthetized with 2.0% (0.1 L/min) of isoflurane delivered in 100% oxygen for 30–60 s. Then the level of isoflurane was maintained between 1.0–1.25% throughout the entire setup and imaging session, during which the respiratory rates were monitored continuously and sustained between 20–30 beats per minute by adjusting isoflurane levels between the range. Placed prone on custom-size plastic bed with a respiratory pad placed underneath the abdomen, body temperatures of the mice were maintained using a warm air recirculation system (SA Instruments, Inc., New York). The head and incisors of mice were secured on the front end of the plastic bed to minimize motion. The front half of the bed was aligned and clamped inside the quad RF coil and placed inside the isocenter of the scanner. Images were acquired using a T1 - weighted spin echo pulse sequence with the following parameters: repetition time (TR)= 300 ms, echo time (TE) = 12 ms, field of view = 19.2 × 19.2, slice thickness = 0.8 mm, 12 slices. Total scan time per mouse was 30 min.

Histology

Six adult *Btbd9* KO mice and 7 WT littermates, or 2 adult *Btbd9* cKO mice and 4 control littermates were anesthetized and perfused with 0.1 M phosphate-buffered saline (pH 7.4; PBS) followed by 4% paraformaldehyde in 0.1 M PBS. The brains were soaked in the paraformaldehyde-PBS at 4°C overnight and soaked in 30% sucrose in 0.1 M PBS until they sank. The brains were frozen by dry-ice powder and cut coronally into 40 μm sections with a Histoslide 2000 sliding microtome (Reichert-Jung) (Yokoi et al., 2009). Sections were rinsed, mounted, and dipped in freshly prepared cresyl violet stain at room temperature for 16 min. After dehydrated with progressively more concentrated ethanol and clarified with xylene, sections were coverslipped with DPX Mountant for histology. Neurolocida was used for the measurements. The magnification used was 10× for ocular lenses and 2.5× for objective lenses. Measurements of the S1HL, M1 and the corpus callosum thickness were made in two planes. The positions of the two planes were (1) between 4.42 and 3.94 mm/interaural reference (anterior), *Btbd9* KO, n = 33 sections for S1HL, n = 64 sections for M1 and n = 57 sections for corpus callosum; WT, n = 44 sections for S1HL, n = 56 sections for M1 and n = 54 sections for corpus callosum; *Btbd9* cKO, n = 18 sections for the S1HL, n = 29 sections for the M1 and n = 20 sections for the corpus callosum; control, n = 44 sections for the S1HL, n = 86 sections for the M1 and n = 46 sections for the corpus callosum, and (2) from 3.82 to 2.58 mm/interaural reference (posterior), *Btbd9* KO, n = 67 sections for S1HL, n = 93 sections for M1 and n = 85 sections for corpus callosum; WT, n = 83 sections for S1HL, n = 110 sections for M1 and n = 119 sections for corpus callosum; *Btbd9* cKO, n = 64 sections for the S1HL, n = 58 sections for M1 and n = 78 sections for the corpus callosum; control, n = 124 sections for the S1HL, n = 132 sections for M1 and n = 131 sections for the corpus callosum.

Whole-cell voltage-clamp recording

Five adult *Drd1-EGFP Btbd9* KO (male: n=2; female: n=3) and 6 *Drd1-EGFP* littermates (male: n=2; female: n=4) with an average age of 2 months were sacrificed, and their brains were rapidly removed. Coronal corticostriatal slices were used for recording spontaneous postsynaptic currents (sEPSC) for 5 mins and evoked currents from EGFP-positive MSNs. Recordings were done in the whole-cell voltage-clamp (MSN neurons were held at −70 mV) configuration, with Cesium methane sulfonate-based internal solution (in mM): 125 Cesium methane sulfonate, 8 NaCl, 10 HEPES, 4 MgATP, 0.3 NaGTP,0.2 EGTA, 0.1% Biocytin, pH 7.2. Picrotoxin (50μM; GABAa receptor blocker) was added in the artificial cerebrospinal fluid (ACSF). Paired-pulse ratios were measured by a glass electrode (3–5 MΩ) filled with the ACSF, which was placed in the white matter around 40 μm away from the recorded region to evoke currents. Currents were obtained from the dorsal-lateral striatal MSNs close to the white matter. The position of the glass electrode was carefully adjusted so as not to evoke polysynaptic responses. Two pulses (20 Hz) were given 10 times for every 10 s with 50 ms inter-pulse interval.

Quantitative real time-PCR (qRT-PCR)

qRT-PCR was performed as described before (Yokoi et al., 2015) to confirm whether exon 4 was deleted in the *Btbd9* cKO mice after *cre*-mediated recombination. In brief, 3 adult *Btbd9* cKO mice and 3 littermates were sacrificed, and brain regions including the cerebral cortex, cerebellum, and spinal cord were harvested and flash frozen in liquid nitrogen. RNA was extracted using an RNAeasy Mini kit (Qiagen) according to the manufacturer's instructions. Next, cDNA was made using SuperScript III reverse transcriptase (Invitrogen). PCR primers specific to *Btbd9* exons 4 and 5 (forward: GAC TCT TGT CTC CGG ATG CT; reverse: TCA CAA CCT GAG CCC CAT AC) and β-actin (forward: CAC CCG CGA GCA CAG CTT CTT TG; reverse: AAT ACA GCC CGG GGA GCA TCG TC) were used. The CFX real-time system was programmed in the following way: 50°C for 2 min, 95°C for 2 min, 50 cycles of 95°C for 30 s, and 65°C for 1 min + plate read, followed by the melting curve analysis: melt curve 65°C to 95°C, increment 0.5°C for 5 s + plate read.

Behavioral studies

30 min open field—Sixteen adult *Btbd9* cKO mice and 14 control littermates were used in the open field analysis as previously described (Yokoi et al., 2008). Briefly, each mouse was placed in the center of a VersaMax Legacy open field apparatus connected to a computerized Digiscan System (Accuscan Instruments, Inc. OH) and continuously monitored for 30 min. Bright illumination (approximately 1 k lux at the center by a 60 W white bulb) was focused on the center of each field.

Continuous open field—A separate batch of four adult *Btbd9* cKO mice and 8 control littermates was monitored under 12 LD for 7 ½ days. As described previously (Lyu et al., 2019a; Lyu et al., 2019b; Meneely et al., 2018), each mouse was placed in the center of a VersaMax Legacy open field apparatus with enough corncob bedding, food, and water. The apparatus contains infrared sensors along the walls that detect any breaks in the beams, which are then decoded by VERSDATA version 2.70–127E (AccuScan Instruments INC.)

into behavioral patterns. The data was recorded every 15 min (15 min bin) throughout the experiment. Data from the first three days were excluded from analysis because the animals were assumed to be accommodating. To compare the total distance traveled between *Btbd9* cKO and WT, we separated the data into a light cycle or dark cycle because mice are nocturnal. Each cycle contains 4–5 periods, from day 4 to day 8, or night 4 to night 7. The distance traveled during each period was added up from the 15 min bins. To compare the probability of waking between the two groups, we recoded the data according to the total distance traveled during each 15 min bin. If the total distance traveled during the 15 min was 0, the mouse was considered as sleeping, and the data were coded as 0; otherwise, the mouse was considered as awake, and the data were coded as 1.

Wheel running—Sixteen adult *Btbd9* cKO mice and 14 control littermates (after the open field test) were monitored under 12 LD condition for 7 days. Wheel running activity was recorded as the number of wheel revolutions occurring during 5 min bins and analyzed using Lafayette Instrument Activity Wheel Monitor software. The activities from the 5th to the 7th day were included in the data analysis, grouped by the light and dark cycles.

Tail flick—Sixteen adult *Btbd9* cKO mice and 14 control littermates (after the wheel running test) were tested for the perception of warm stimuli using the Tail Flick Analgesia Meter (San Diego Instruments) as previously described (DeAndrade et al., 2012a). Briefly, each mouse was placed in an acrylic restrainer with the distal end of its tail protruding under a heat lamp. The lamp, together with a timer, was turned on, both of which stopped automatically when the mouse flicked its tail away from the light. The latency to respond was limited to 15 s to prevent injury to the mouse.

Rotarod and beam walking—Eight *Btbd9* KO mice and 9 WT littermates and the third batch of 5 *Btbd9* cKO mice and 6 control littermates were tested as described previously (Dang et al., 2005). The apparatus started at an initial speed of 4 rpm and gradually accelerated at a rate of 0.2 rpm/s. The latency to fall was measured with a cutoff time of 3 min. Mice were tested for three trials on each day for 2 days. The trials within the same day were performed approximately 1 h apart.

After resting for a week, animals were trained to traverse a medium square beam (14 mm wide) in three consecutive trials each day for 2 days. After training was completed, the experiment commenced with recordings of the number of hind paw slips for each of the two trials per beam. On the first test day, animals were made to cross the medium square and round beam (17 mm diameter) and on the second day, a small round beam (10 mm diameter) and an additional small square beam (7 mm wide). Any animal dropped during the test was assigned the largest number observed during the whole beam walking experiment.

Data processing and statistical analysis

Images were processed and analyzed as previously reported (Perez et al., 2013). Mn^{2+} accumulation in active neurons produces signal intensity increases in T1 images. However, as this is a non-quantitative approach to measure activity and because there is scan-to-scan intensity variation independent of Mn^{2+}, we normalized images based on their individual

variance (Perez et al., 2013). Using this normalization approach, where surpassing a normalized threshold value of 1 indicates increased activity associated with Mn^{2+} administration, we have observed significant differences between Mn^{2+} administered and non-treated rodents. Image processing was carried out using ITK-SNAP (http://www.itksnap.org) and image math scripts were available on FSL (fslmaths http://www.fmrib.ox.ac.uk/fsl/). Scans were aligned with a segmented atlas of the adult mouse brain using an automated affine linear registration tool from FSL (Jenkinson et al., 2012). Each scan was converted to a z value map through a voxel-wise normalization procedure. The mean signal intensity across the entire extracted brain volume (x^{-}) was subtracted from each voxel (xi) and then divided by the variance (σ). A pre-set threshold of $z \geq 1$ was selected based on a prior observation of individual datasets and a close inspection of their intensity distribution histograms. All voxels with z score values below this threshold were set to zero. Thus, the voxels exceeding the threshold value of $z \geq 1$ were considered in our statistical analysis as having higher signal intensities (quantified as the number of voxels above a z value of 1). The mean number of voxels for each region of interest (ROI) was compared using an unpaired two-tailed t-test (homoscedastic variances, $\alpha \leq 0.05$).

The data were tested for normality using the SPSS statistical package first. Part of the thickness of specific brain region, PPF, membrane properties, wheel running test, continuous open field, tail-flick data and rotarod data for *Btbd9* KO were not normally distributed and were analyzed by the logistic regression with a gamma distribution (SAS statistical package), which log-transformed the data and then normalized the WT or the control group to 0 without the error bar. 30 min open field activity, the sEPSC, the rest of the cortical thickness data and rotarod data for *Btbd9* cKO were normally distributed and compared by mixed-model ANOVA (SAS). Beam walking data were count data hence were analyzed by logistic regression with a negative binomial distribution. Gender (if females were used) and age were used as covariates in both ANOVA and logistic regression. qRT-PCR data were analyzed by the Student's t-test.

Results

Increased cortical but decreased hippocampal neural activity in the *Btbd9* KO mice

After image normalization and setting a z-score threshold ≥ 1, we observed the signal intensity of Mn^{2+} uptake in various regions of interest (ROI) for both *Btbd9* KO mice and their WT littermates (Figure 1A). These ROIs were further parceled into smaller subsections for subsequent qualitative inspection of neural activity. In the cerebral cortical region, the number of activated voxels was most significantly increased in the primary somatosensory cortex (S1) and the rostral piriform cortex (PirR) (Figure 1B, $p < 0.05$). These brain areas are involved in processing sensations like touch (Bolognini et al., 2013), proprioception (Kim et al., 2015), nociception (Bushnell et al., 1999), temperature (Moulton et al., 2012) and smell (Bekkers and Suzuki, 2013). In addition, we found a significantly decreased neural activity in the dentate gyrus (DG) of the hippocampus. The hippocampus belongs to the allocortex, which is the other subtype of cortex except for the neocortex (Creutzfeldt, 1995). The DG receives most of the inputs from the entorhinal cortex (EntCtx) and projects to Schaffer collateral CA3 and then to CA1 (Amaral et al., 2007). Therefore, the decreased

neural activity in DG here is consistent with the previous data showing that *Btbd9* KO mice have a significantly reduced CA3 to CA1 synaptic neurotransmission in the form of enhanced long-term potentiation (DeAndrade et al., 2012b).

Decreased cortical thickness in the S1HL and M1 of the *Btbd9* KO mice

RLS patients exhibit decreased thickness in S1 and the corpus callosum (Lee et al., 2018). Accordingly, we measured the thickness of S1 and the corpus callosum in the *Btbd9* KO mice. We found that the *Btbd9* KO mice did not have changes in the thickness of the corpus callosum (Figure 2D, anterior, $p = 0.84$; posterior, $p = 0.22$) compared with their WT littermates. However, *Btbd9* KO mice had reduced cortical thickness in the anterior S1HL region (Figure 2B, anterior, $p = 0.02$; 13% reduction) but not in the posterior S1HL region (Figure 2B, posterior, $p = 0.95$). In the WT, the thickness of S1HL generally decreased from the anterior to the posterior parts (data not shown). However, *Btbd9* KO mice maintained the same thickness in S1HL across the sections. This result resembles the clinical finding and may be responsible for the sensory deficit found in the *Btbd9* KO mice (Allen et al., 2017; DeAndrade et al., 2012a; DeAndrade and Li, 2015). In addition, we also found decreased thickness in the anterior part of the M1 (Figure 2C, anterior, $p = 0.0004$; 13% reduction), but not in the posterior part of the M1 (Figure 2C, posterior, $p = 0.76$) in the *Btbd9* KO mice.

Corticostriatal synaptic neurotransmission in the *Btbd9* KO mice

The iron deprived rats, which is thought to be an RLS rodent model, show elevated corticostriatal excitability (Yepes et al., 2017). Here, part of the M1 in *Btbd9* KO mice showed morphological changes. To investigate if the output of the motor cortex to the striatum was influenced by the loss of BTBD9, we performed the whole-cell voltage-clamp recording. MSNs comprise ~95% of the neurons in the striatum. D1 MSNs, which form the direct pathway and account for around half of the MSNs, are thought to be involved in movement facilitation and pronociceptive sensation (Albin et al., 1995; Barcelo et al., 2012). We compared the PPF between the *Btbd9* KO mice and their WT littermates by recording from D1 MSNs and found a significantly increased PPF (Figure 3B, $p = 0.02$) in the mutant mice, which suggest enhanced short-term plasticity at the corticostriatal terminals to D1 MSNs. Although there was no change in the postsynaptic sEPSC of D1 MSNs (Figure 3D, $p = 0.64$; Figure 3E, $p = 0.64$; Figure 3F, $p = 0.87$; Figure 3G, $p = 0.92$), the mutant mice showed a significantly higher membrane resistance (Figure 3, the table, $p = 0.03$). The results suggest that in the mutant mice, the spontaneous release of the neurotransmitter was normal, and the mutant D1 MSNs have less opened channels. Both our data and the iron deprived rat study imply a functional alteration at corticostriatal synapses in RLS animal models.

Generation and confirmation of the *Btbd9* cKO mice

To find out if the BTBD9 mutation in the cerebral cortex alone is sufficient for the development of behavioral and morphological alterations like RLS patients, we generated the *Btbd9* cKO mice using the *cre-loxP* system (Figure 4A). We used qRT-PCR and found that the expression of the *Btbd9* was specifically decreased in the cerebral cortex (Figure 4B, $p = 0.02$), without altering the expression in the cerebellum (Figure 4B, $p = 0.26$) and the spinal cord (Figure 4B, $p = 0.38$). It should be noticed that the remaining expression of

Btbd9 may be due to the inputs from other parts of the brain and non-glutamatergic neurons (Guo et al., 2000; Kummer et al., 2012).

Motor restlessness, sleep disturbance and decreased thermal sensation in the *Btbd9* cKO mice

The diagnostic criteria described in the International Restless Legs Syndrome Study Group include an urge to move the legs, which are partially or totally relieved by movement (Garcia Borreguero et al., 2017). Previous *Btbd9* KO mouse and fruit fly models of RLS have shown increased activity levels (DeAndrade et al., 2012a; Freeman et al., 2012). Therefore, we utilized an open field chamber and the wheel running assembly to assess the total and voluntary activity levels of the *Btbd9* cKO mice. In the 30 min open field test, we found that the *Btbd9* cKO mice exhibited a similar level of total distance traveled compared with the control group (Figure 5A, left panel, $p = 0.14$). Clockwise and counterclockwise circling, which are linked to balance in DA system (Kim et al., 2000; Viggiano et al., 2003), were also found to be the same between the *Btbd9* cKO mice and the controls (Figure 5A, right panel, CW, $p = 0.42$; CCW, $p = 0.05$). Wheel running study indicated that the voluntary activity levels of *Btbd9* cKO mice were similar to the control group both during the light phase (Figure 5B, left panel, $p = 0.51$), when the animals are normally sleeping or resting, and during the dark phase (Figure 5B, right panel, $p = 0.70$), when the animals are usually active. In the continuous open field test, *Btbd9* cKO showed a significant increase in their activity level during the light phase (Figure 5C, left panel, $p = 0.02$) but not during the dark phase (Figure 5C, right panel, $p = 0.48$). In addition, sleep analysis indicates an increased probability of waking of the *Btbd9* cKO mice in the light phase (Figure 5D, left panel, $p = 0.04$) but not in the dark phase (Figure 5D, right panel, $p = 0.44$). The results suggest that the *Btbd9* cKO mice had significantly increased rest-phase activity. Loss of the BTBD9 protein only in the cerebral cortex can lead to a circadian-dependent motor restlessness.

Another critical feature of RLS is paraesthesia of the legs (Allen et al., 2014; Ondo and Jankovic, 1996; Yeh et al., 2016). *Btbd9* KO mice showed increased thermal sensation (DeAndrade et al., 2012a). Therefore, we tested the sensory system of the *Btbd9* cKO mice using the tail-flick test. The mutant mice had a lower level of sensitivity to the heat stimuli compared with the control group (Figure 5E, $p = 0.008$), indicating that loss of BTBD9 only in the cerebral cortex can lead to alterations in sensory perception.

Impaired motor function in both *Btbd9* KO and *Btbd9* cKO mice

Given the decreased thickness found in a part of the M1, motor functions of *Btbd9* KO mice were tested by both rotarod and beam walking tests. Rotarod test reveals the animal's gross motor ability to maintain balance and coordination while they are challenged by the instability of a rotating rod, while beam walking test poses challenges to the subject's fine motor balance and coordination skills (Dang et al., 2005). We found that *Btbd9* KO mice showed decreased latency to fall in the rotarod test (Figure 5F, left panel, $p = 0.0093$) and had a 228% increase of slips in the beam walking test (Figure 5G, left panel, $p < 0.0001$), indicating that the motor function of *Btbd9* KO mice was impaired. We also tested the *Btbd9* cKO mice. Interestingly, although *Btbd9* cKO mice did not show deficit in the rotarod test (Figure 5F, right panel, $p = 0.90$), they had a 219% increase of slips in the beam walking test

(Figure 5G, right panel, $p = 0.0057$), suggesting that the loss of BTBD9 only in the cerebral cortex is sufficient to cause motor deficit.

Decreased cortical thickness in the S1HL and M1 of the *Btbd9* cKO mice

In the *Btbd9* KO mice, the decreased thickness of S1HL and M1 was companied by changes found in both sensory and motor behavioral tests. Considering the similar behavioral alterations of *Btbd9* cKO mice, we measured the thickness of S1HL and M1 in the *Btbd9* cKO mice with the same method. We found that *Btbd9* cKO mice had thinner cortical layers in both the anterior and posterior S1HL regions (Figure 6B, anterior, $p = 0.003$; 7% reduction; posterior, $p = 0.0008$; 9% reduction), and the posterior M1 regions (Figure 6C, posterior, $p = 0.04$; 4% reduction). The thickness in the anterior M1 regions (Figure 6B, anterior, $p = 0.17$) and the corpus callosum (Figure 6D, anterior, $p = 0.84$; posterior, $p = 0.18$) were not altered. The morphological changes were quite similar between the *Btbd9* KO and *Btbd9* cKO mice.

Discussion

In this study, we determined how the loss of *Btbd9* affects the function and morphometry of the cerebral cortex and focused on the role of corticostriatal synapses in RLS pathogenesis. Our results demonstrated that: (1) In the somatosensory pathway, *Btbd9* KO had increased neural activities in the S1 and reduced thickness in the anterior part of the S1HL; (2) In the motor pathway, *Btbd9* KO mice had reduced thickness in the anterior part of the M1 and increased PPF in the corticostriatal pathway to D1 MSNs. Furthermore, *Btbd9* KO mice demonstrated motor deficits in both rotarod and beam walking tests; (3) Sole BTBD9 deficiency in the cerebral cortex is sufficient to cause a decrease in the thickness of S1HL and M1, RLS-like phenotypes and motor deficits. The study has limitations. We did not explore the interaction between S1 and M1, while in RLS patients, sensorimotor integration is likely affected (Tyvaert et al., 2009). Nevertheless, the results presented here highlight the importance of the cerebral cortex, especially the S1 and M1, in the pathogenesis of RLS. Functional alteration of corticostriatal synapses may be the underlying mechanism for the development of RLS.

Systematic BTBD9 deficiency led to enhanced neural activity in the S1 but reduced thickness in part of the S1. S1 plays a critical role in processing afferent somatosensory input from both the body periphery and the external environment (Borich et al., 2015). The change in cortical thickness here is consistent with a recent clinical study showing that the S1 of human RLS patients has similar morphologic alterations (Lee et al., 2018). Concurrent with the structural changes in the somatosensory cortex and pathway (Lee et al., 2018), RLS patients have an altered central sensitization process in reflex and sensory tests (Nitsche and Paulus, 2000; Paulus et al., 2007; Schattschneider et al., 2004; Stiasny-Kolster et al., 2013). Similarly, decreased somatosensory cortical thickness in *Btbd9* KO mice is accompanied by increased sensitivity to the heat stimuli (DeAndrade et al., 2012a), which may be associated with the increased S1 neural activity as observed in the MEMRI study.

Systematic BTBD9 deficiency did not cause neural activity changes in M1, but led to a decreased thickness in the anterior part of M1, increased PPF in the corticostriatal pathway

to D1 MSNs and motor deficits. Neurophysiologic studies with RLS patients suggest increased excitability in the motor cortical neurons (Bocquillon et al., 2017; Salas et al., 2018). Although *Btbd9* KO mice did not show neural activity changes in M1, they had increased neural activity in S1. It has been known that communication between somatosensory and motor areas and sensorimotor integration are important for the acquisition and performance of motor skills (Arce-McShane et al., 2016). Inputs from the sensory cortex participate in motor learning and retention of the learned motor skills. Focal lesions of sensorimotor areas have resulted in motor deficits in animal models (Brinkman et al., 1985; Gerlai et al., 2000; Hikosaka et al., 1985; Kleim et al., 2007). Therefore, neural activity change in S1 may contribute to the motor deficits observed in *Btbd9* KO mice. In addition, decreased thickness in the anterior part of M1 and increased PPF in the corticostriatal pathway may also contribute to the abnormal behavioral output. Specifically, increased PPF implies a lower probability of synaptic vesicle release, a larger neurotransmitter pool for subsequent external stimulation and enhanced short-term plasticity at D1 corticostriatal synapses. Previously, iron-deprived rats show hyperactive corticostriatal nerve terminals (Yepes et al., 2017). The result is consistent with ours and suggests a functional augmentation of the motor corticostriatal synapses to D1 MSNs. D1 MSNs are thought to be pronociceptive and facilitate movement (Albin et al., 1995; Barcelo et al., 2012). Altered activity in D1-mediated pathway here is consistent with the increased locomotor and sensory outputs found in *Btbd9* KO and iron-deprived animals (DeAndrade et al., 2012a; Dowling et al., 2009; Qu et al., 2007).

It should be noticed that the hippocampal Schaffer collateral CA3-CA1 pyramidal neurons, which use glutamate as its neurotransmitter, also show increased PPF in the *Btbd9* KO mice comparing to WT mice (DeAndrade et al., 2012b). Therefore, the enhanced short-term plasticity or the impaired synaptic vesicle release caused by a loss of BTBD9 function seems to be a common phenotype in these presynaptic glutamatergic terminals. The impaired glutamate release from these presynaptic terminals may transmit abnormal excitatory signals and affect the downstream neuronal circuits in the corresponding brain regions, which contribute to the behavioral phenotypes.

Cerebral cortex-specific *Btbd9* mutation is sufficient to cause decreased cortical thickness, RLS-like phenotypes, and motor deficits. The symptoms of RLS patients begin or become worse at night or in the evening. One of the previous genetic mouse models of RLS, *Meis1* KO mice, showed increased activity level throughout the day and night (Meneely et al., 2018). *PTPRD* homozygous KO mice were found to show 22% decrease in sleep as measured by video taken in for the hour before and the hour after lights off (Drgonova et al., 2015). Here, *Btbd9* cKO mice exhibited an increased activity level and the probability of waking only during the light phase. Since mice have opposite circadian rhythms as humans, *Btbd9* cKO resembled the circadian rhythm-dependent hyperactivity of RLS patients. In addition, RLS patients show hypersensitivity to a pinprick as well as tactile hypoesthesia and dysesthesia to non-noxious cold stimuli (paradoxical heat sensation) (Stiasny-Kolster et al., 2004; Stiasny-Kolster et al., 2013). Also, RLS patients show hyperalgesia to blunt pressure and hyperaesthesia to vibration (Bachmann et al., 2010). *Btbd9* cKO mice had sensory changes similar to RLS patients in that they showed an increased latency to warm stimuli. Finally, RLS patients were found to have decreased thickness of the S1 (Lee et al., 2018).

We confirmed that both *Btbd9* KO mice and *Btbd9* cKO mice had thinner S1HL. The decrease in somatosensory cortical thickness, therefore, may be correlated with the sensory deficit. *Btbd9* KO mice and *Btbd9* cKO mice also had thinner M1. They both showed impaired motor behaviors in the rotarod and bema walking tests. Hence the decrease in primary cortical thickness may be correlated with the motor deficits.

Our finding demonstrated a decreased neural activity in DG but increased neural activity in PirR of the *Btbd9* KO mice. DG receives excitatory inputs from the EntCtx (Witter, 2007). Although the *p*-value did not reach the significant, the neural activity of EntCtx showed a decrease in the KO (Figure 1B), which is consistent with the decreased neural activity in DG. The output from DG projects to CA3 (Jonas and Lisman, 2014). Therefore, the lower neural activity in DG is consistent with our previous finding showing that the *Btbd9* KO mice had an enhanced long-term potentiation in the CA3-CA1 pathway (DeAndrade et al., 2012b). PirR receives inputs from olfactory bulbs and connects to the amygdala. PirR is thought to be involved in the sense of smell (Bekkers and Suzuki, 2013). Disturbances in the olfactory system of RLS patients have not been reported in the past. However, patients with Parkinson's disease (PD) often have a significant olfactory loss (Haehner et al., 2014). A recent study indicates that RLS may be associated with two premotor symptoms of the PD (Iwaki et al., 2018). Hence, we speculate that the activity change here may be another sign of PD development. It should be noticed that the volume of the olfactory bulb constitutes only 0.01% of humans brain (Morfometría Comparada Del Bulbo, 2011). Different from humans, rodents have a huge olfactory bulb relative to their overall brain size. Therefore, this change in PirR can also be rodent-specific.

Conclusions

Our findings support the idea that systematic loss of BTBD9 in mice can lead to enhanced neural activity in S1, a decreased thickness in the anterior parts of S1 and M1, an increased PPF in the D1 corticostriatal pathway and motor deficits. Cerebral cortical BTBD9 deficiency alone is sufficient to induce both behavioral and morphological phenotypes resembling *Btbd9* KO mice.

Supplementary Material

Refer to Web version on PubMed Central for supplementary material.

Acknowledgments

Authors acknowledge the support from the National High Magnetic Field Laboratory's Advanced Magnetic Resonance Imaging & Spectroscopy (AMRIS) Facility (National Science Foundation Cooperative Agreement No. DMR-1157490 and the State of Florida). We thank Dr. David Lovinger and his lab members for helping with brain slice recording.

Formatting of funding sources

This work was supported by the National Institutes of Health [grants NS082244, NS065273] and the Restless Legs Syndrome Foundation.

Abbreviations

12 LD	12-hour light, 12-hour dark
***Btbd9* cKO**	cerebral cortex-specific *Btbd9* knockout mice
***Btbd9* KO**	*Btbd9* homozygous knockout mice
CCW	counterclockwise
CW	clockwise
DG	dentate gyrus
EntCtx	entorhinal cortex
GEE	generalized estimating equation
GWAS	genome-wide association studies
KO	knockout
M1	primary motor cortex
MEMRI	manganese-enhanced magnetic resonance imaging
MSN	medium spiny neuron
PirR	rostral piriform cortex
PLMS	periodic limb movement of sleep
PPF	paired-pulse facilitation
qRT-PCR	Quantitative real time-PCR
RLS	restless leg syndrome
ROI	region of interest
S1	primary somatosensory cortex
S1HL	primary somatosensory cortex representing the hindlimb
sEPSC	spontaneous excitatory postsynaptic currents
WT	wild type

References:

Albin RL, Young AB, Penney JB, 1995 The functional anatomy of disorders of the basal ganglia. Trends Neurosci 18, 63–64. [PubMed: 7537410]

Allen RP, Donelson NC, Jones BC, Li Y, Manconi M, Rye DB, Sanyal S, Winkelmann J, 2017 Animal models of RLS phenotypes. Sleep Med 31, 23–28. [PubMed: 27839945]

Allen RP, Picchietti DL, Garcia-Borreguero D, Ondo WG, Walters AS, Winkelman JW, Zucconi M, Ferri R, Trenkwalder C, Lee HB, 2014 Restless legs syndrome/Willis-Ekbom disease diagnostic

criteria: updated International Restless Legs Syndrome Study Group (IRLSSG) consensus criteria--history, rationale, description, and significance. Sleep Med 15, 860–873. [PubMed: 25023924]

Amaral DG, Scharfman HE, Lavenex P, 2007 The dentate gyrus: fundamental neuroanatomical organization (dentate gyrus for dummies). Prog Brain Res 163, 3–22. [PubMed: 17765709]

Arce-McShane FI, Ross CF, Takahashi K, Sessle BJ, Hatsopoulos NG, 2016 Primary motor and sensory cortical areas communicate via spatiotemporally coordinated networks at multiple frequencies. Proc Natl Acad Sci U S A 113, 5083–5088. [PubMed: 27091982]

Bachmann CG, Rolke R, Scheidt U, Stadelmann C, Sommer M, Pavlakovic G, Happe S, Treede RD, Paulus W, 2010 Thermal hypoaesthesia differentiates secondary restless legs syndrome associated with small fibre neuropathy from primary restless legs syndrome. Brain 133, 762–770. [PubMed: 20194142]

Barcelo AC, Filippini B, Pazo JH, 2012 The striatum and pain modulation. Cell Mol Neurobiol 32, 1–12. [PubMed: 21789630]

Bekkers JM, Suzuki N, 2013 Neurons and circuits for odor processing in the piriform cortex. Trends Neurosci 36, 429–438. [PubMed: 23648377]

Bocquillon P, Charley-Monaca C, Houdayer E, Marques A, Kwiatkowski A, Derambure P, Devanne H, 2017 Reduced afferent-induced facilitation of primary motor cortex excitability in restless legs syndrome. Sleep Med 30, 31–35. [PubMed: 28215259]

Bolognini N, Rossetti A, Convento S, Vallar G, 2013 Understanding others' feelings: the role of the right primary somatosensory cortex in encoding the affective valence of others' touch. J Neurosci 33, 4201–4205. [PubMed: 23447627]

Borich MR, Brodie SM, Gray WA, Ionta S, Boyd LA, 2015 Understanding the role of the primary somatosensory cortex: Opportunities for rehabilitation. Neuropsychologia 79, 246–255. [PubMed: 26164474]

Brinkman J, Colebatch JG, Porter R, York DH, 1985 Responses of precentral cells during cooling of post-central cortex in conscious monkeys. J Physiol 368, 611–625. [PubMed: 4078751]

Bucher SF, Seelos KC, Oertel WH, Reiser M, Trenkwalder C, 1997 Cerebral generators involved in the pathogenesis of the restless legs syndrome. Ann Neurol 41, 639–645. [PubMed: 9153526]

Bushnell MC, Duncan GH, Hofbauer RK, Ha B, Chen JI, Carrier B, 1999 Pain perception: is there a role for primary somatosensory cortex? Proc Natl Acad Sci U S A 96, 7705–7709. [PubMed: 10393884]

Celle S, Roche F, Peyron R, Faillenot I, Laurent B, Pichot V, Barthelemy JC, Sforza E, 2010 Lack of specific gray matter alterations in restless legs syndrome in elderly subjects. J Neurol 257, 344–348. [PubMed: 19768657]

Chang Y, Chang HW, Song H, Ku J, Earley CJ, Allen RP, Cho YW, 2015 Gray matter alteration in patients with restless legs syndrome: a voxel-based morphometry study. Clin Imaging 39, 20–25. [PubMed: 25176196]

Comley RA, Cervenka S, Palhagen SE, Panagiotidis G, Matthews JC, Lai RY, Halldin C, Farde L, Nichols TE, Whitcher BJ, 2012 A comparison of gray matter density in restless legs syndrome patients and matched controls using voxel-based morphometry. J Neuroimaging 22, 28–32. [PubMed: 21091816]

Connor JR, Ponnuru P, Lee BY, Podskalny GD, Alam S, Allen RP, Earley CJ, Yang QX, 2011 Postmortem and imaging based analyses reveal CNS decreased myelination in restless legs syndrome. Sleep Med 12, 614–619. [PubMed: 21570342]

Creutzfeldt OO, 1995 Cortex cerebri : performance, structural, and functional organization of the cortex / O.D. Creutzfeldt

Dang MT, Yokoi F, McNaught KS, Jengelley TA, Jackson T, Li J, Li Y, 2005 Generation and characterization of Dyt1 DeltaGAG knock-in mouse as a model for early-onset dystonia. Exp Neurol 196, 452–463. [PubMed: 16242683]

DeAndrade MP, Johnson RL Jr., Unger EL, Zhang L, van Groen T, Gamble KL, Li Y, 2012a Motor restlessness, sleep disturbances, thermal sensory alterations and elevated serum iron levels in Btbd9 mutant mice. Hum Mol Genet 21, 3984–3992. [PubMed: 22678064]

DeAndrade MP, Li Y, 2015 Chapter 80 - Btbd9 Knockout Mice as a Model of Restless Legs Syndrome, in: LeDoux MS (Ed.), Movement Disorders (Second Edition). Academic Press, Boston, pp. 1191–1205.

DeAndrade MP, Zhang L, Doroodchi A, Yokoi F, Cheetham CC, Chen HX, Roper SN, Sweatt JD, Li Y, 2012b Enhanced hippocampal long-term potentiation and fear memory in Btbd9 mutant mice. PLoS One 7, e35518. [PubMed: 22536397]

Dowling P, Klinker F, Amaya F, Paulus W, Liebetanz D, 2009 Iron-deficiency sensitizes mice to acute pain stimuli and formalin-induced nociception. J Nutr 139, 2087–2092. [PubMed: 19776188]

Drgonova J, Walther D, Wang KJ, Hartstein GL, Lochte B, Troncoso J, Uetani N, Iwakura Y, Uhl GR, 2015 Mouse model for PTPRD associations with WED/RLS and addiction: reduced expression alters locomotion, sleep behaviors and cocaine-conditioned place preference. Mol Med.

Etgen T, Draganski B, Ilg C, Schroder M, Geisler P, Hajak G, Eisensehr I, Sander D, May A, 2005 Bilateral thalamic gray matter changes in patients with restless legs syndrome. Neuroimage 24, 1242–1247. [PubMed: 15670702]

Ferre S, Garcia-Borreguero D, Allen RP, Earley CJ, 2019 New Insights into the Neurobiology of Restless Legs Syndrome. Neuroscientist 25, 113–125. [PubMed: 30047288]

Freeman A, Pranski E, Miller RD, Radmard S, Bernhard D, Jinnah HA, Betarbet R, Rye DB, Sanyal S, 2012 Sleep fragmentation and motor restlessness in a Drosophila model of Restless Legs Syndrome. Curr Biol 22, 1142–1148. [PubMed: 22658601]

Garcia Borreguero D, Winkelmann J, Allen RP, 2017 Introduction: Towards a better understanding of the science of RLS/WED. Sleep Med 31, 1–2. [PubMed: 27894926]

Gerlai R, Thibodeaux H, Palmer JT, van Lookeren Campagne M, Van Bruggen N, 2000 Transient focal cerebral ischemia induces sensorimotor deficits in mice. Behav Brain Res 108, 63–71. [PubMed: 10680758]

Guo H, Hong S, Jin XL, Chen RS, Avasthi PP, Tu YT, Ivanco TL, Li Y, 2000 Specificity and efficiency of Cre-mediated recombination in Emx1-Cre knock-in mice. Biochem Biophys Res Commun 273, 661–665. [PubMed: 10873661]

Haehner A, Hummel T, Reichmann H, 2014 A clinical approach towards smell loss in Parkinson's disease. J Parkinsons Dis 4, 189–195. [PubMed: 24322062]

Hikosaka O, Tanaka M, Sakamoto M, Iwamura Y, 1985 Deficits in manipulative behaviors induced by local injections of muscimol in the first somatosensory cortex of the conscious monkey. Brain Res 325, 375–380. [PubMed: 3978429]

Hornyak M, Ahrendts JC, Spiegelhalder K, Riemann D, Voderholzer U, Feige B, van Elst LT, 2007 Voxel-based morphometry in unmedicated patients with restless legs syndrome. Sleep Med 9, 22–26. [PubMed: 17512782]

Iwaki H, Hughes KC, Gao X, Schwarzschild MA, Ascherio A, 2018 The association between restless legs syndrome and premotor symptoms of Parkinson's disease. J Neurol Sci 394, 41–44. [PubMed: 30212740]

Jenkinson M, Beckmann CF, Behrens TE, Woolrich MW, Smith SM, 2012 FSL. Neuroimage 62, 782–790. [PubMed: 21979382]

Jonas P, Lisman J, 2014 Structure, function, and plasticity of hippocampal dentate gyrus microcircuits. Front Neural Circuits 8, 107. [PubMed: 25309334]

Khan FH, Ahlberg CD, Chow CA, Shah DR, Koo BB, 2017 Iron, dopamine, genetics, and hormones in the pathophysiology of restless legs syndrome. J Neurol 264, 1634–1641. [PubMed: 28236139]

Kim DS, Szczypka MS, Palmiter RD, 2000 Dopamine-deficient mice are hypersensitive to dopamine receptor agonists. J Neurosci 20, 4405–4413. [PubMed: 10844009]

Kim SS, Gomez-Ramirez M, Thakur PH, Hsiao SS, 2015 Multimodal Interactions between Proprioceptive and Cutaneous Signals in Primary Somatosensory Cortex. Neuron 86, 555–566. [PubMed: 25864632]

Kleim JA, Boychuk JA, Adkins DL, 2007 Rat models of upper extremity impairment in stroke. Ilar j 48, 374–384. [PubMed: 17712223]

Kummer M, Kirmse K, Witte OW, Holthoff K, 2012 Reliable in vivo identification of both GABAergic and glutamatergic neurons using Emx1-Cre driven fluorescent reporter expression. Cell Calcium 52, 182–189. [PubMed: 22658827]

Lee BY, Kim J, Connor JR, Podskalny GD, Ryu Y, Yang QX, 2018 Involvement of the central somatosensory system in restless legs syndrome: A neuroimaging study. Neurology.

Lyu S, DeAndrade MP, Mueller S, Oksche A, Walters AS, Li Y, 2019a Hyperactivity, dopaminergic abnormalities, iron deficiency and anemia in an in vivo opioid receptors knockout mouse: Implications for the restless legs syndrome. Behav Brain Res 374, 112123. [PubMed: 31376441]

Lyu S, Xing H, DeAndrade MP, Liu Y, Perez PD, Yokoi F, Febo M, Walters AS, Li Y, 2019b The role of BTBD9 in striatum and restless legs syndrome. eNeuro.

Margariti PN, Astrakas LG, Tsouli SG, Hadjigeorgiou GM, Konitsiotis S, Argyropoulou MI, 2012 Investigation of unmedicated early onset restless legs syndrome by voxel-based morphometry, T2 relaxometry, and functional MR imaging during the night-time hours. AJNR Am J Neuroradiol 33, 667–672. [PubMed: 22173758]

Meneely S, Dinkins M-L, Kassai M, Lyu S, Liu Y, Lin C-T, Brewer K, Li Y, Clemens S, 2018 Differential dopamine D1 and D3 receptor modulation and expression in the spinal cord of two mouse models of Restless Legs Syndrome. Frontiers in Behavioral Neuroscience 12.

Morfometría Comparada Del Bulbo TE, Olfatoria Humano, Perro Y Cabra, Boniface M. Kavoi, Hassanali Jameela, 2011 Comparative Morphometry of the Olfactory Bulb, Tract and Stria in the Human, Dog and Goat. Int. J. Morphol 29, 939–946.

Moulton EA, Pendse G, Becerra LR, Borsook D, 2012 BOLD responses in somatosensory cortices better reflect heat sensation than pain. J Neurosci 32, 6024–6031. [PubMed: 22539862]

Nitsche MA, Paulus W, 2000 Excitability changes induced in the human motor cortex by weak transcranial direct current stimulation. J Physiol 527 Pt 3, 633–639. [PubMed: 10990547]

Ondo W, Jankovic J, 1996 Restless legs syndrome: clinicoetiologic correlates. Neurology 47, 1435–1441. [PubMed: 8960723]

Pan PL, Dai ZY, Shang HF, Xiao PR, Dong CS, Song WG, Zhou GL, Zhong JG, Shi HC, 2014 Gray matter anomalies in anterior cingulate cortex as a correlate of depressive symptoms in drug-naive idiopathic restless legs syndrome. Neuroscience 277, 1–5. [PubMed: 24993478]

Paulus W, Dowling P, Rijsman R, Stiasny-Kolster K, Trenkwalder C, de Weerd A, 2007 Pathophysiological concepts of restless legs syndrome. Mov Disord 22, 1451–1456. [PubMed: 17516488]

Perez PD, Hall G, Kimura T, Ren Y, Bailey RM, Lewis J, Febo M, Sahara N, 2013 In vivo functional brain mapping in a conditional mouse model of human tauopathy (tauP301L) reveals reduced neural activity in memory formation structures. Mol Neurodegener 8, 9. [PubMed: 23379588]

Qu S, Le W, Zhang X, Xie W, Zhang A, Ondo WG, 2007 Locomotion is increased in a11-lesioned mice with iron deprivation: a possible animal model for restless legs syndrome. J Neuropathol Exp Neurol 66, 383–388. [PubMed: 17483695]

Salas RME, Kalloo A, Earley CJ, Celnik P, Cruz TE, Foster K, Cantarero G, Allen RP, 2018 Connecting clinical aspects to corticomotor excitability in restless legs syndrome: a TMS study. Sleep Medicine.

San Pedro EC, Mountz JM, Mountz JD, Liu HG, Katholi CR, Deutsch G, 1998 Familial painful restless legs syndrome correlates with pain dependent variation of blood flow to the caudate, thalamus, and anterior cingulate gyrus. J Rheumatol 25, 2270–2275. [PubMed: 9818676]

Scalise A, Cadore IP, Gigli GL, 2004 Motor cortex excitability in restless legs syndrome. Sleep Med 5, 393–396. [PubMed: 15222998]

Scalise A, Pittaro-Cadore I, Janes F, Marinig R, Gigli GL, 2010 Changes of cortical excitability after dopaminergic treatment in restless legs syndrome. Sleep Med 11, 75–81. [PubMed: 19595629]

Schattschneider J, Bode A, Wasner G, Binder A, Deuschl G, Baron R, 2004 Idiopathic restless legs syndrome: abnormalities in central somatosensory processing. J Neurol 251, 977–982. [PubMed: 15316803]

Schormair B, Zhao C, Bell S, Tilch E, Salminen AV, Putz B, Dauvilliers Y, Stefani A, Hogl B, Poewe W, Kemlink D, Sonka K, Bachmann CG, Paulus W, Trenkwalder C, Oertel WH, Hornyak M, Teder-Laving M, Metspalu A, Hadjigeorgiou GM, Polo O, Fietze I, Ross OA, Wszolek Z, Butterworth AS, Soranzo N, Ouwehand WH, Roberts DJ, Danesh J, Allen RP, Earley CJ, Ondo WG, Xiong L, Montplaisir J, Gan-Or Z, Perola M, Vodicka P, Dina C, Franke A, Tittmann L, Stewart AFR, Shah SH, Gieger C, Peters A, Rouleau GA, Berger K, Oexle K, Di Angelantonio E,

Hinds DA, Muller-Myhsok B, Winkelmann J, 2017 Identification of novel risk loci for restless legs syndrome in genome-wide association studies in individuals of European ancestry: a meta-analysis. Lancet Neurol 16, 898–907. [PubMed: 29029846]

Stiasny-Kolster K, Magerl W, Oertel WH, Moller JC, Treede RD, 2004 Static mechanical hyperalgesia without dynamic tactile allodynia in patients with restless legs syndrome. Brain 127, 773–782. [PubMed: 14985260]

Stiasny-Kolster K, Pfau DB, Oertel WH, Treede RD, Magerl W, 2013 Hyperalgesia and functional sensory loss in restless legs syndrome. Pain 154, 1457–1463. [PubMed: 23707286]

Stogios PJ, Downs GS, Jauhal JJ, Nandra SK, Prive GG, 2005 Sequence and structural analysis of BTB domain proteins. Genome Biol 6, R82. [PubMed: 16207353]

Tyvaert L, Houdayer E, Devanne H, Bourriez JL, Derambure P, Monaca C, 2009 Cortical involvement in the sensory and motor symptoms of primary restless legs syndrome. Sleep Med 10, 1090–1096. [PubMed: 19427261]

Unrath A, Juengling FD, Schork M, Kassubek J, 2007 Cortical grey matter alterations in idiopathic restless legs syndrome: An optimized voxel-based morphometry study. Mov Disord 22, 1751–1756. [PubMed: 17566123]

Unrath A, Muller HP, Ludolph AC, Riecker A, Kassubek J, 2008 Cerebral white matter alterations in idiopathic restless legs syndrome, as measured by diffusion tensor imaging. Mov Disord 23, 1250–1255. [PubMed: 18464282]

Viggiano D, Ruocco LA, Sadile AG, 2003 Dopamine phenotype and behaviour in animal models: in relation to attention deficit hyperactivity disorder. Neurosci Biobehav Rev 27, 623–637. [PubMed: 14624807]

Winkelmann J, Schormair B, Lichtner P, Ripke S, Xiong L, Jalilzadeh S, Fulda S, Putz B, Eckstein G, Hauk S, Trenkwalder C, Zimprich A, Stiasny-Kolster K, Oertel W, Bachmann CG, Paulus W, Peglau I, Eisensehr I, Montplaisir J, Turecki G, Rouleau G, Gieger C, Illig T, Wichmann HE, Holsboer F, Muller-Myhsok B, Meitinger T, 2007 Genome-wide association study of restless legs syndrome identifies common variants in three genomic regions. Nat Genet 39, 1000–1006. [PubMed: 17637780]

Witter MP, 2007 The perforant path: projections from the entorhinal cortex to the dentate gyrus. Prog Brain Res 163, 43–61. [PubMed: 17765711]

Yeh P, Ondo WG, Picchietti DL, Poceta JS, Allen RP, Davies CR, Wang L, Shi Y, Bagai K, Walters AS, 2016 Depth and Distribution of Symptoms in Restless Legs Syndrome/ Willis-Ekbom Disease. J Clin Sleep Med 12, 1669–1680. [PubMed: 27655450]

Yepes G, Guitart X, Rea W, Newman AH, Allen RP, Earley CJ, Quiroz C, Ferre S, 2017 Targeting hypersensitive corticostriatal terminals in restless legs syndrome. Ann Neurol 82, 951–960. [PubMed: 29171915]

Yokoi F, Dang MT, Liu J, Gandre JR, Kwon K, Yuen R, Li Y, 2015 Decreased dopamine receptor 1 activity and impaired motor-skill transfer in Dyt1 DeltaGAG heterozygous knock-in mice. Behav Brain Res 279, 202–210. [PubMed: 25451552]

Yokoi F, Dang MT, Miller CA, Marshall AG, Campbell SL, Sweatt JD, Li Y, 2009 Increased c-fos expression in the central nucleus of the amygdala and enhancement of cued fear memory in Dyt1 DeltaGAG knock-in mice. Neurosci Res 65, 228–235. [PubMed: 19619587]

Yokoi F, Dang MT, Mitsui S, Li J, Li Y, 2008 Motor deficits and hyperactivity in cerebral cortex-specific Dyt1 conditional knockout mice. J Biochem 143, 39–47. [PubMed: 17956903]

Yue F, Cheng Y, Breschi A, Vierstra J, Wu W, Ryba T, Sandstrom R, Ma Z, Davis C, Pope BD, Shen Y, Pervouchine DD, Djebali S, Thurman RE, Kaul R, Rynes E, Kirilusha A, Marinov GK, Williams BA, Trout D, Amrhein H, Fisher-Aylor K, Antoshechkin I, DeSalvo G, See LH, Fastuca M, Drenkow J, Zaleski C, Dobin A, Prieto P, Lagarde J, Bussotti G, Tanzer A, Denas O, Li K, Bender MA, Zhang M, Byron R, Groudine MT, McCleary D, Pham L, Ye Z, Kuan S, Edsall L, Wu YC, Rasmussen MD, Bansal MS, Kellis M, Keller CA, Morrissey CS, Mishra T, Jain D, Dogan N, Harris RS, Cayting P, Kawli T, Boyle AP, Euskirchen G, Kundaje A, Lin S, Lin Y, Jansen C, Malladi VS, Cline MS, Erickson DT, Kirkup VM, Learned K, Sloan CA, Rosenbloom KR, Lacerda de Sousa B, Beal K, Pignatelli M, Flicek P, Lian J, Kahveci T, Lee D, Kent WJ, Ramalho Santos M, Herrero J, Notredame C, Johnson A, Vong S, Lee K, Bates D, Neri F, Diegel M, Canfield T, Sabo PJ, Wilken MS, Reh TA, Giste E, Shafer A, Kutyavin T, Haugen E, Dunn D,

Reynolds AP, Neph S, Humbert R, Hansen RS, De Bruijn M, Selleri L, Rudensky A, Josefowicz S, Samstein R, Eichler EE, Orkin SH, Levasseur D, Papayannopoulou T, Chang KH, Skoultchi A, Gosh S, Disteche C, Treuting P, Wang Y, Weiss MJ, Blobel GA, Cao X, Zhong S, Wang T, Good PJ, Lowdon RF, Adams LB, Zhou XQ, Pazin MJ, Feingold EA, Wold B, Taylor J, Mortazavi A, Weissman SM, Stamatoyannopoulos JA, Snyder MP, Guigo R, Gingeras TR, Gilbert DM, Hardison RC, Beer MA, Ren B, 2014 A comparative encyclopedia of DNA elements in the mouse genome. Nature 515, 355–364. [PubMed: 25409824]

Highlights

- *Btbd9* knockout (KO) mice had increased excitability in primary sensory cortex.
- *Btbd9* KO mice had decreased cortical thickness in part of the S1 and M1.
- *Btbd9* KO mice showed increased corticostriatal PPF and motor deficits.
- Cerebral cortex-specific *Btbd9* KO mice (*Btbd9* cKO) had RLS-like phenotypes.
- *Btbd9* cKO showed decreased thickness in part of the S1 and M1 and motor deficits.

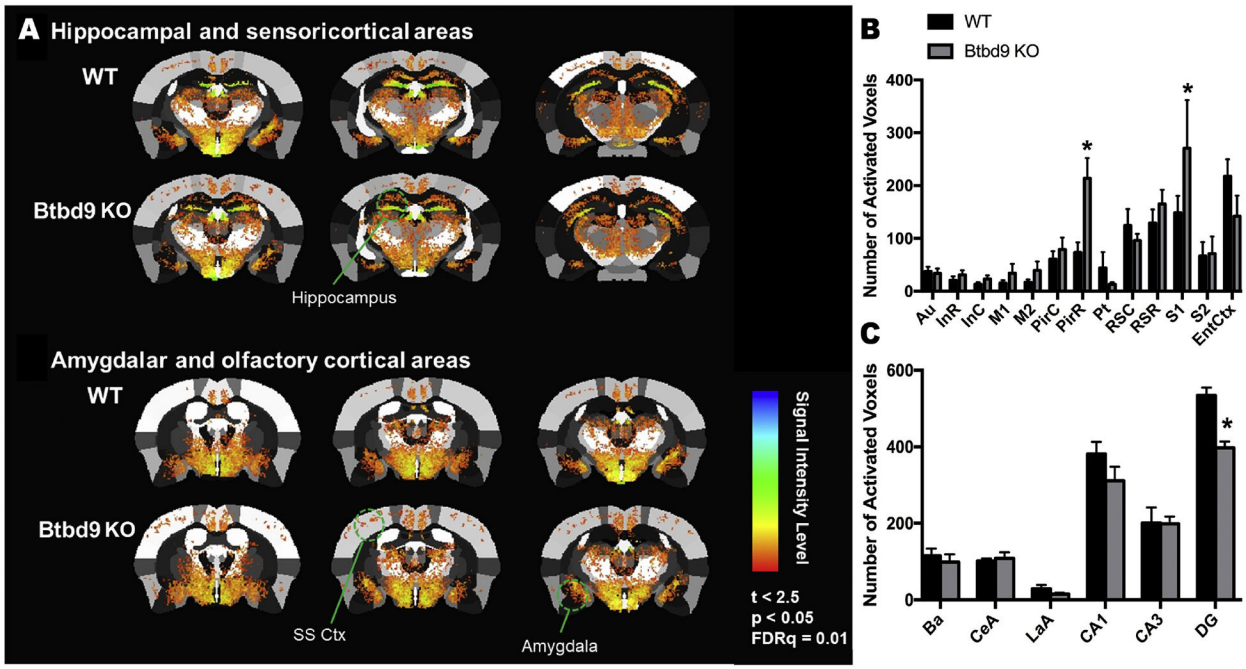

Figure 1.

MEMRI recordings of neural activity in the cerebral cortex of 6 *Btbd9* KO males and 7 WT male littermates. (A) Coronal views of the averaged signal intensity from *Btbd9* KO and WT mice. (B) *Btbd9* KO had increased neural activity in S1 and PirR. No difference was observed in other cerebral cortical regions like the motor cortex. (C) *Btbd9* KO showed decreased neural activity in hippocampal DG. Bars represent means plus standard errors (SEs). *, $p < 0.05$. Au: auditory cortex; Ba: basal amygdala; CA1: *Cornu Ammonis* 1; CA3: *Cornu Ammonis* 3; CeA: central nucleus of the amygdala; DG: dentate gyrus; EntCtx: entorhinal cortex; InC: caudal insular cortex; InR: rostral insular cortex; LaA: lateral amygdala; M1: primary motor cortex; M2: secondary motor cortex; PirC: caudal piriform cortex; PirR: rostral piriform cortex; Pt: posterior parietal association area; RSC: caudal retrosplenial cortex; RSR: rostral neutropenia cortex; S1: primary somatosensory cortex; S2: secondary somatosensory cortex.

*Color needed for print.

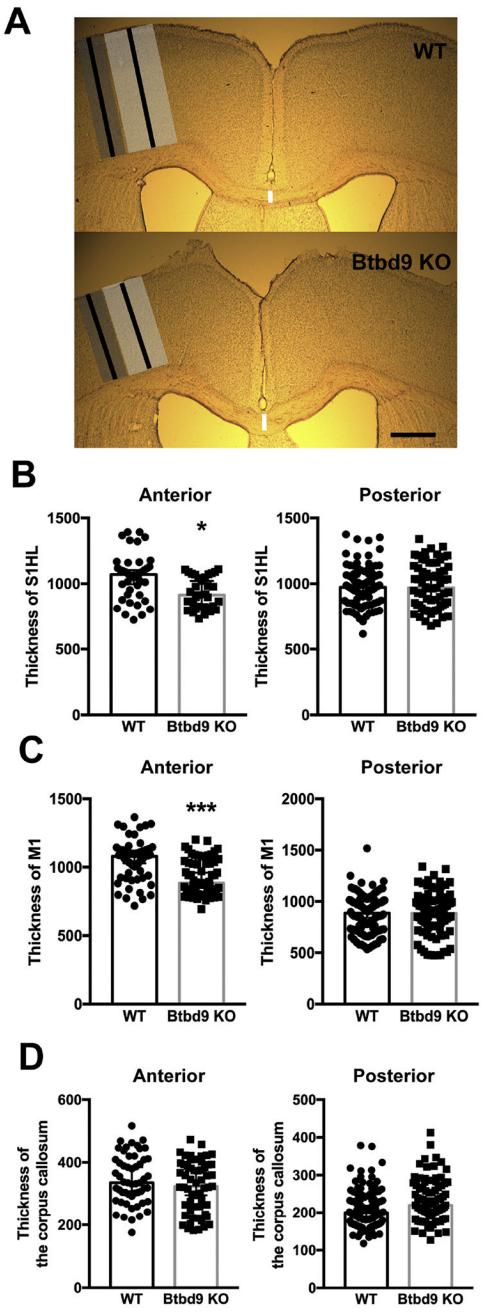

Figure 2.

The thickness of the primary somatosensory cortex, primary motor cortex and corpus callosum from 6 *Btbd9* KO males and 7 WT male littermates. (A) Representative coronal views of brain slices (Atlas, interaural 3.94 mm) from a *Btbd9* KO mouse and its WT littermate, respectively. The areas under the dark gray shed are the primary somatosensory cortex representing the hindlimb (S1HL). The areas under the light gray shed are the primary motor cortex (M1). The black lines are where measurements of S1HL and M1 were made and the white vertical lines show where the thickness of the corpus callosum was compared. Scale bars: 500 μm. (B) The anterior (*Btbd9* KO, n=33 sections; WT, n=40

sections) but not the posterior (*Btbd9* KO, n=67 sections; WT, n=83 sections) part of the S1HL of *Btbd9* KO showed a 13% decrease in the thickness. (C) The anterior (*Btbd9* KO, n=64 sections; WT, n=56 sections) but not the posterior (*Btbd9* KO, n=93 sections; WT, n=110 sections) part of the M1 of *Btbd9* KO showed a 13% decrease in the thickness. (D) Both the anterior (*Btbd9* KO, n=57 sections; WT, n=54 sections) and the posterior (*Btbd9* KO, n=85 sections; WT, n=119 sections) parts of the corpus callosum of *Btbd9* KO were unchanged in the thickness. Data are presented as median with 95% confident interval (CI). ***, $p < 0.005$; *, $p < 0.05$.

*No color needed for print.

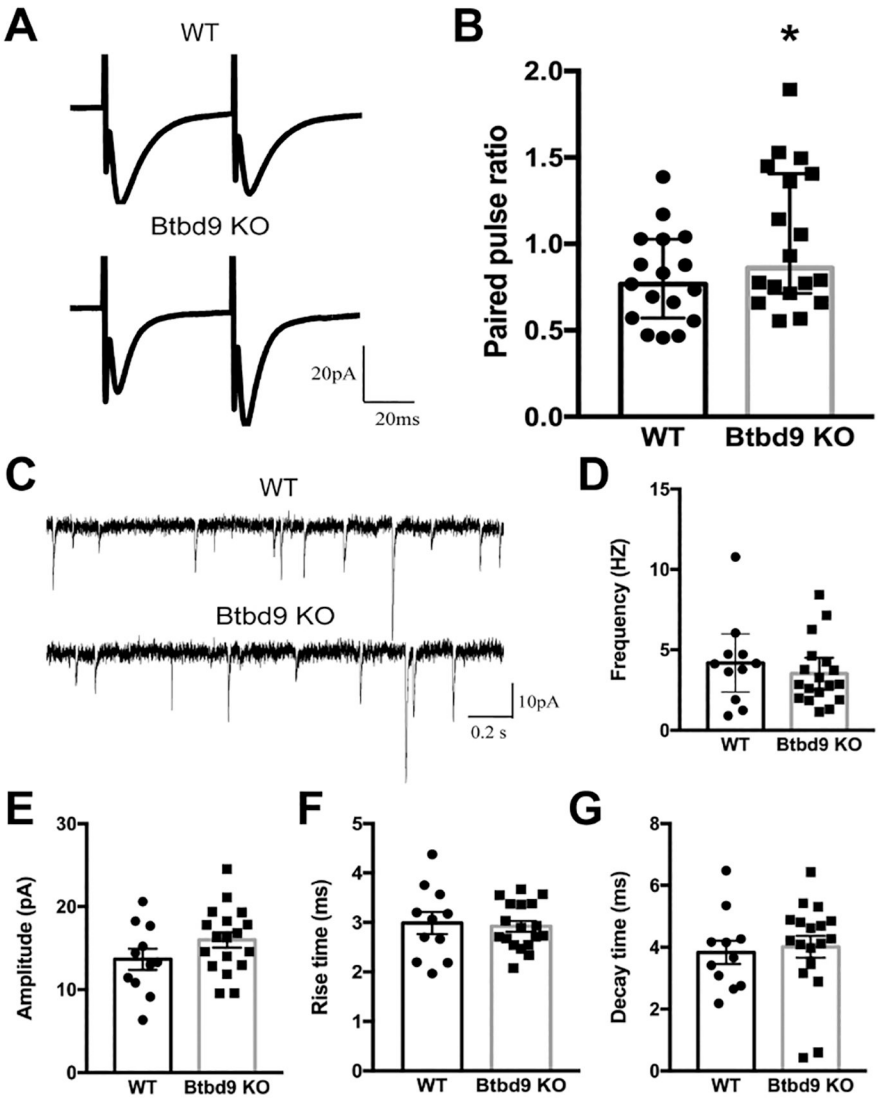

D1 MSNs	Membrane capacitance (pF)			Membrane resistance (MΩ)			Time constant (ms)		
	Average	SE	*p*	Average	SE	*p*	Average	SE	*p*
WT (n = 21)	105.62	5.33	0.79	140.86	14.61	0.03*	1.98	0.12	0.73
Btbd9 KO (n = 20)	101.95	6.86		184.65	21.21		1.86	0.12	

Figure 3.

Whole-cell voltage-clamp recording from 5 *Drd1-EGFP Btbd9* KO and 6 *Drd1-EGFP* WT littermates. (A) Representative traces of paired-pulse facilitation (PPF) at the inter-pulse interval of 50 ms from the WT and the *Btbd9* KO. (B) *Btbd9* KO mice showed increased PPF. Data were log-transformed and the WT group was normalized to 0 without the error bar (see method). 17 cells from WT and 18 cells from KO mice were analyzed, cells were nested under animals in statistical analysis. Bars represent means plus SEs. (C) Representative sEPSC traces of D1 MSNs from the WT and the *Btbd9* KO. (D) The frequency of spontaneous firing of D1 MSNs was similar between the *Btbd9* KO and the WT groups. (E) *Btbd9* KO D1 MSNs had the same amplitude of sEPSC as the WT. (F, G) Both the rise and decay times were not different between the *Btbd9* KO and WT D1 MSNs.

Data are presented as median with 95% CI. The table at the bottom presents membrane properties of D1 MSNs. *, $p < 0.05$.

*No color needed for print.

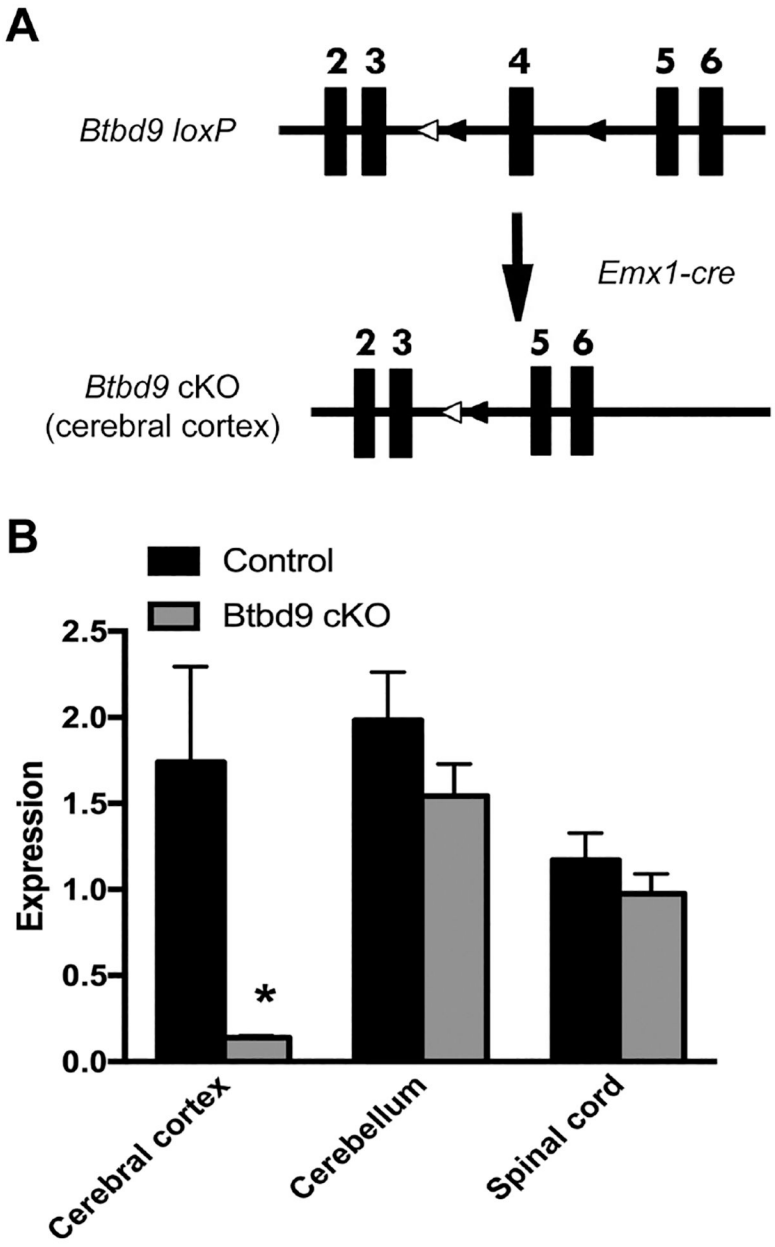

Figure 4.

Quantitative real time-PCR with 3 *Btbd9* cKO males and their 3 male littermates. (A) Schematic diagram of the generation of the *Btbd9* cKO mice. Filled boxes represent exons. Filled triangles indicate *loxP* sites. Open triangles indicate the *FRT* sites that were incorporated to remove the neo cassette. In *Btbd9* cKO mice, exon 4 is deleted in the cerebral cortex because *cre* is expressed specifically in the cerebral cortex. The recombination occurs in the cortical cells, while other brain regions and the rest of the body still retain the intact exons. (B) *Btbd9* cKO mice showed a decreased level of *Btbd9* mRNA in the cerebral cortex compared to the controls. Bars represent the means plus SEs. *, $p < 0.05$.

*No color needed for print.

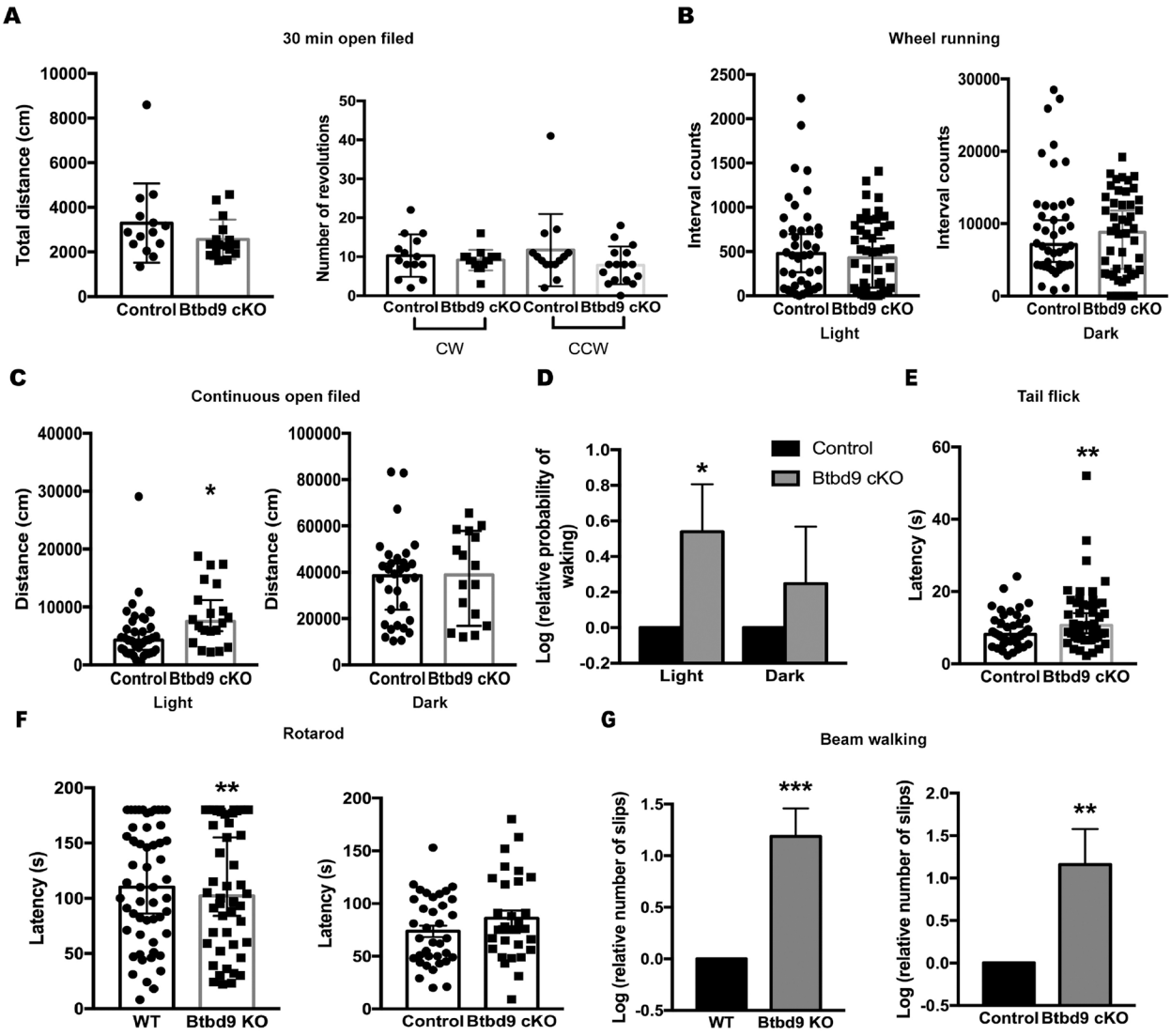

Figure 5.

Behavioral tests of *Btbd9* cKO mice and their control littermates. (A) *Btbd9* cKO mice (n=16) traveled a similar amount of distance when compared with controls (n=14) in a 30 min open field test. The circling activities of *Btbd9* cKO mice were at the same level as controls. (B) Wheel running activity was the same between *Btbd9* cKO (n=16, 3 days and 3 nights) and control mice (n=14, 3 days and 3 nights) both during the light and the dark phases. (C) In the continuous open field test, *Btbd9* cKO mice (n=4, 4 days and 3 nights) showed a significant increase in the total distance traveled during the light phase, but not during the dark phase compared with the controls (n=8, 4 days and 3 nights). (D) *Btbd9* cKO (n=4) showed an increased probability of waking in the light phase of the continuous open field test compared with the controls (n=8). (E) *Btbd9* cKO mice (n=16, 3 repeats) showed an increased latency for the heat stimuli in the tail-flick test compared with the controls (n=14, 3 repeats). (F) *Btbd9* KO mice (n=8, 6 trials), compared with their wild-type littermates (n=9, 6 trials), had decreased latency to fall in the rotarod test. *Btbd9* cKO mice (n=5, 6 trials) did not show motor deficits in the test compared with their controls (n=6, 6

trials). (G) Both *Btbd9* KO and *Btbd9* cKO mice showed increased number of slips in the beam walking test. Bars in figure A, D, right panel of F and G represent means plus SEs. Data in figure B, C, E and left panel of F are presented as median with 95% CI. Data in figure D were analyzed by the binominal logistic regression with GEE model and data in figure G were analyzed by the negative binomial logistic regression with GEE model (see method), which log-transformed the data and normalized the control groups to 0 without the error bar. *** $p < 0.005$; **, $p < 0.01$; *, $p < 0.05$.
*No color needed for print.

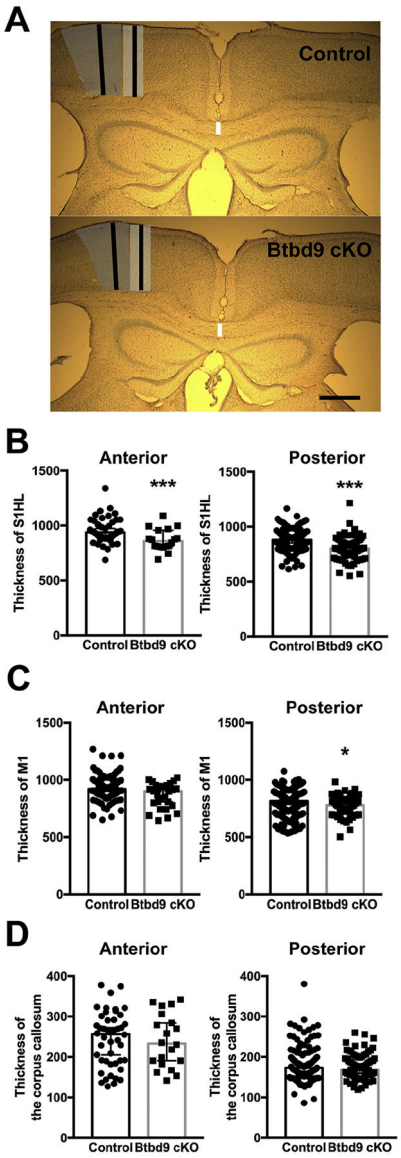

Figure 6.

The thickness of the primary somatosensory cortex, primary motor cortex and corpus callosum from 2 *Btbd9* cKO mice and their 4 control littermates. (A) Representative coronal views of brain slices (Mouse Brain Atlas, interaural 2.74 mm) from a *Btbd9* cKO mouse and its control littermate, respectively. The areas under the dark gray shed are the primary somatosensory cortex representing the hindlimb (S1HL). The areas under the light gray shed are the primary motor cortex (M1). The black lines are where measurements of S1HL and M1 were made and the white vertical lines show where the thickness of the corpus callosum was compared. Scale bars: 500 μm. (B) Both anterior (*Btbd9* cKO, n=18 sections; Control, n=44 sections) and posterior (*Btbd9* cKO, n=64 sections; Control, n=124 sections) S1HL of *Btbd9* cKO showed a decrease in the thickness (anterior, 7% reduction; posterior, 9% reduction). (C) Posterior (*Btbd9* cKO, n=58 sections; Control, n=132 sections), but not the anterior (*Btbd9* cKO, n=29 sections; Control, n=86 sections) M1 of *Btbd9* cKO showed a

decrease in the thickness (posterior, 4% reduction). (D) Neither the anterior *Btbd9* cKO, n=20 sections; Control, n=46 sections) nor the posterior *Btbd9* cKO, n=78 sections; Control, n=131 sections) corpus callosum of *Btbd9* cKO had decreased in the thickness. Data are presented as median with 95% CI. ***, $p < 0.005$; *, $p < 0.05$.

*No color needed for print.